EurJIC
European Journal of Inorganic Chemistry

Research Article
doi.org/10.1002/ejic.202500224

Chemistry Europe
European Chemical Societies Publishing

www.eurjic.org

Platinum-Binding Peptides: Binding Kinetics, Affinities, and Facet-Specific Conformational Adaptation

Monika Michaelis,* Marion J. Limo, Swetha R. Kothur, and Carole C. Perry*

Platinum-binding peptides (PtBPs) identified via phage display have emerged as powerful molecular tools for the controlled synthesis and functionalization of nanostructured platinum surfaces. However, the molecular determinants governing their surface recognition, binding strength, and structural adaptability remain incompletely understood. Here, a comparative analysis of five PtBPs, three previously reported (TLTTLTN, SSFPQPN, TLHVSSY) and two newly identified by phage display (TGELSQK, LLVTSVT), using quartz crystal microbalance with dissipation monitoring (QCM-D) and synchrotron radiation circular dichroism (SRCD) spectroscopy, is presented. Adsorption kinetics and binding affinities determined by QCM-D reveal sequence-specific differences in association and dissociation rates, which correlate with the viscoelastic properties of the adsorbed layers. SRCD spectra show that all peptides adopt predominantly disordered conformations in solution but exhibit facet-dependent spectral shifts upon adsorption onto platinum nanoparticles, consistent with conformational adaptation at the interface. The combined data highlight the importance of amino acid composition, kinetic binding parameters, and conformational flexibility in governing Pt–PtBP interactions. This integrated approach provides a deeper understanding of peptide–surface recognition and may support the rational design of sequence-defined biomolecules for use in catalysis, surface modification, and biomedical nanotechnology.

1. Introduction

The inevitable depletion of fossil fuel reserves and rising energy demands, coupled with environmental pollution, have driven the development of sustainable materials and technologies.[1,2] Platinum (Pt), a precious transition metal, is particularly attractive due to its excellent electrical properties, outstanding catalytic activity and stability, and superior corrosion resistance.[3,4] Pt remains a leading choice for important industrial reactions such as methanol oxidation,[5] hydrogen oxidation,[6] oxygen reduction,[7] and hydrogenation,[8,9] as well as biomedical applications.[10,11] Recent efforts have focused on developing sustainable methods to synthesize Pt nanoparticles with controlled physicochemical properties—especially morphology (size and shape)—given its critical influence on performance in these applications.[12,13]

Diverse fabrication methods have been developed for the synthesis of Pt nanomaterials, but solution-based routes involving the reduction or decomposition of metal precursors are particularly attractive. These methods allow for precise control over nanoparticle nucleation, growth, and aging by adjusting parameters such as solution composition and reaction temperature.[3,14–16] At a fundamental level, nanocrystal nucleation and growth are governed by kinetic and thermodynamic parameters, as crystal formation in solution is driven by the minimization of the system's total free energy.[17] Pt nanoparticles adopt a face-centered-cubic (fcc) symmetry, and their low-index crystal planes exhibit different surface energies[18] to reduce the overall surface energy. Pt nanocrystals typically expose low-index facets—most commonly {111}, {100}, and {110}, in order of increasing surface energy.[13,18] Single-crystalline morphologies such as cubes, tetrahedra, octahedra, and their truncated forms are common, though the presence of defects can lead to more complex or lower-symmetry shapes, including hexagonal and triangular plates, nanorods, planar tripods, and multipods.[13,15,18] Morphological control and stabilization are often achieved using structure-directing agents (SDAs), such as surfactants, inorganic species, polymers, and biomolecules. These SDAs adsorb onto growing nanocrystals and modulate the relative surface energies of different facets, thereby directing crystal growth.[19–26] Among these, proteins and peptides have garnered particular interest due to their recognition capabilities, sequence specificity, self-assembly behavior, and biofabrication potential under green synthesis conditions.[27–32]

The Nobel-prize awarded phage display (PD) technique[33–35] has been successfully applied to identify peptides that can bind to a broad spectrum of commercially relevant materials, both biotic and abiotic.[36–42] Platinum-binding peptides (PtBPs) identified by this or related methods have demonstrated remarkable versatility in directing the synthesis and structural control of Pt nanoparticles.[16,20,23,43] In all reported Pt mineralization studies, control reactions conducted without PtBPs consistently yielded aggregated nanocrystals with broad particle size distributions.[16,20,23,43]

M. Michaelis, M. J. Limo, S. R. Kothur, C. C. Perry
Biomolecular and Materials Interface Research Group
Interdisciplinary Biomedical Research Centre
School of Science and Technology
Nottingham Trent University
Clifton Lane, Nottingham NG11 8NS, UK
E-mail: michaelis@uni-bremen.de
carole.perry@ntu.ac.uk

Supporting information for this article is available on the WWW under https://doi.org/10.1002/ejic.202500224

Specific PtBPs have been shown to modulate either the nucleation[20,43] or growth phase[23,43] of nanoparticle formation. For instance, the TLHVSSY peptide is believed to influence nucleation by stabilizing twinned seeds, while TLTTLTN and SSFPQPN are thought to guide growth through facet-specific preferential binding behavior.[23,43,44] Despite these promising applications, the molecular mechanisms underpinning Pt–PtBP interfacial interactions remain not fully understood, particularly in terms of how amino acid composition, binding kinetics and affinities, and structural adaptability contribute to peptide adsorption and surface recognition.[38,44–46]

Several experimental and computational techniques, including instance surface plasmon resonance, fluorometric peptide assays, and molecular dynamics (MD) simulations, have been employed to investigate Pt–PtBP interactions.[7,38,44–46] These studies have focused on characterizing peptide conformation, assessing potential differences between bound and unbound states, and evaluating adsorption behavior, binding affinities, surface coverage, kinetic parameters, and interaction stability. Factors proposed to govern these interactions include the presence of reactive side chains, particularly hydroxyl-rich residues, as well as the peptide's sequence order and conformational flexibility, which may modulate the accessibility of binding motifs.[23,38,45,46]

Circular dichroism spectroscopy studies have shown that the investigated PtBPs generally adopt disordered conformations in solution.[44,46] Conformational instability is a common characteristic of biomolecules involved in solid-surface recognition and binding.[47–51] Such structural flexibility enhances the adaptability to interfacial features, facilitating the presentation of functionally relevant side chains at the binding interface.[47] This intrinsic disorder may also promote conformational changes upon surface interaction, potentially leading to localized structural stabilization.[46,52–54] In some cases, more complex processes, including peptide–peptide interactions and physical recognition of Pt surface topography, may induce conformational reorganization, potentially leading to supramolecular self-assembly at the metal interface.[20,23,38,43,46,55] These insights into conformational flexibility raise further questions about how structural tendencies relate to adsorption behavior across different PtBPs.

While affinity constants and structural insights have been reported for individual PtBPs, systematic side-by-side comparisons of multiple sequences under identical experimental conditions remain limited. Moreover, few studies have combined kinetic and viscoelastic parameters from quartz crystal microbalance with dissipation monitoring (QCM-D) with structural information to correlate adsorption behavior with conformational adaptability. Here, we address this gap by quantitatively comparing five PtBPs, three previously reported (TLHVSSY, TLTTLTN, and SSFPQPN) and two novel sequences identified in-house (TGELSQK and LLVTSVT), using a polycrystalline platinum sensor predominantly exposing the {111} facet. Through the integration of adsorption kinetics, binding affinities, dissipation profiles, and synchrotron radiation circular dichroism (SRCD) spectroscopy, we establish how amino acid composition and intrinsic conformational backbone propensities influence both binding strength and adsorption behavior. This combined approach enhances the mechanistic understanding of PtBP–surface interactions and may inform the rational design of peptide-based SDAs for platinum interfaces in catalysis, sensing, or nanomaterials development.

2. Results and Discussion

2.1. Selection and Sequence Characteristics of Platinum-Binding Peptides

In a first step, we identified two novel platinum binding peptides using PD using two different targets, in-house synthesized platinum nanoparticles, which preferentially display {100} surfaces, and commercial polycrystalline nanoparticle source (see S1a, Supporting Information).

The peptides displayed by the phage clones which were responsive for the screening and selecting for the two different targets were analyzed after the third and fifth round of the biopanning experiments. The sequences of peptides obtained from third and fifth round of biopanning experiments are shown in **Figure 1**b,c. Sequences obtained by the biopanning procedure on the Pt {100} target were analyzed following the same procedure. The analysis of the third and fifth round biopanning experimental peptide sequences was found to have "TGELSQK" consensus sequence (see Figure 1b). For the polycrystalline Pt target the consensus peptide sequence was found to be "LLVTSVT," as represented in Figure 1c. The physicochemical properties of these two novel sequences are compared with other well-known platinum binding peptides in **Table 1**.

The T7 peptide (Ac-TLTTLTN-$CONH_2$) is a well-established platinum-binding sequence, initially identified via PD for its specific affinity toward {100} platinum facets.[23] Studies have demonstrated that T7 selectively stabilizes {100} surfaces, modulating platinum nanocrystal growth to promote the formation of nanocubes.[23] MD simulations further revealed that T7 peptides bind preferentially to the edges and corners of {100} facets, where interactions with platinum atoms are strongest, reducing surface energy and directing crystal growth.[56] T7 has also been used to assemble ultrathin 2D platinum nanoplates, demonstrating that peptide-mediated assembly can be leveraged to control nanostructure formation.[7] Additionally, adsorption studies suggest that T7 binds via hydroxyl residues in threonine and hydrophobic interactions from leucine, which may explain its facet specificity.[57] Stochastic tunneling-basin hopping simulations have confirmed that T7 adopts a more extended conformation when bound to Pt {100}, facilitating the formation of a structured peptide layer on the surface, whereas on Pt {111}, its organization is less ordered.[58]

The S7 peptide (Ac-SSFPQPN-$CONH_2$) was originally identified through PD for its specific affinity toward Pt-{111} facets.[23] Studies have demonstrated that S7 selectively stabilizes {111} surfaces, directing the growth of tetrahedral platinum nanocrystals by inhibiting atom addition along the $<111>$ direction.[44] MD simulations and adsorption studies revealed that S7 binds strongly to Pt-{111} through interactions with phenylalanine (F), glutamine (Q), and asparagine (N), which facilitate hydrogen

Research Article
doi.org/10.1002/ejic.202500224

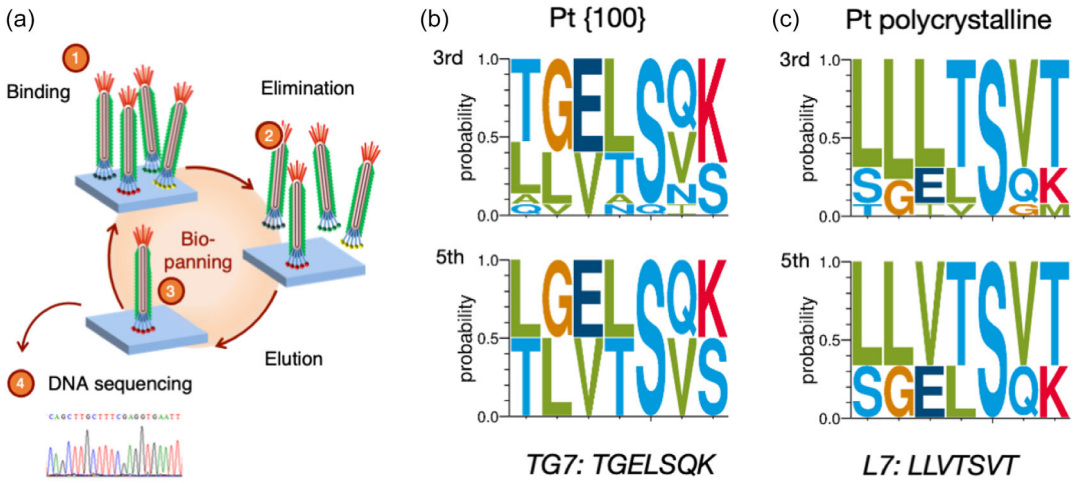

Figure 1. Overview of the biopanning procedure and the obtained results. a) Schematic representation of the steps involved in the biopanning procedure. b,c) Representation of the sequences bound in the 3rd and 5th round of the biopanning to the {100} Pt target and the polycrystalline target, respectively. Representations in (b), (c) were produced via WebLogo 3.5.0.[86,87]

Table 1. Comparison of physicochemical properties of selected PD identified Pt binding peptides.

Sequence	TLTTLTN (T7)	SSFPQPN (S7)	TLHVSSY (BP7A)	TGELSQK (TG7)	LLVTSVT (L7)
Pt target in PD	{100}[23]	{111}[23]	Nanowires[20]	{100}	polycrystalline
Nonpolar uncharged amino acids	LL (29%)	FPP (43%)	LVY (29%)	L (14%)	LLVV (57%)
Polar uncharged amino acids	TTTTN (71%)	SSQN (57%)	TSS (57%)	GTSQ (58%)	TST (43%)
+ve charged amino acids	–	–	H (14%)	K (14%)	–
−ve charged amino acids	–	–	–	E (14%)	–
Hydropathy (GRAVY)[88]	0.186	−1.286	0.171	−1.286	1.971
Calculated net charge[88]	–	–	–	–	–
Isoelectric point (pI)[88]	5.19	5.24	6.40	5.66	5.52

bonding and electrostatic interactions with the Pt surface.[57] Additionally, the hydroxyl groups of serine (S) contribute to its strong binding affinity, distinguishing its adsorption behavior from peptides preferring {100} facets.[57] Further mechanistic studies identified phenylalanine (F) as the dominant motif responsible for S7's specificity toward Pt-{111}, as it promotes selective binding through aromatic interactions while simultaneously reducing affinity for {100} facets.[44] Stochastic tunneling-basin hopping simulations have confirmed that S7 adopts a more compact conformation on Pt-{111}, likely due to the clustering of interacting residues at the interface, whereas on Pt-{100}, its organization appears less ordered.[58]

The BP7a peptide (TLHVSSY) was originally identified through PD using a polycrystalline platinum target, where it was found to influence the nucleation and growth of platinum nanocrystals.[20,59] Further studies demonstrated that BP7a promotes the formation of single-twinned platinum seeds, leading to the development of multipod morphologies during nanoparticle synthesis.[43] MD simulations suggest that BP7a preferentially stabilizes the Pt-{111} facet, a property linked to its ability to direct twinned seed formation at the nucleation stage.[60] The strong binding of histidine (H) to Pt ions plays a critical role in modulating reduction kinetics, slowing the growth rate and promoting structural rearrangements that favor twin-plane formation.[61] Adsorption studies further confirmed that the N-terminal residues TLHV are responsible for nucleation effects, while the C-terminal SSY motif facilitates pod elongation, indicating a sequence-dependent functional division within the peptide.[23] Despite its critical role in Pt nanoparticle synthesis, limited direct information on BP7a's conformation in solution or upon binding is available. However, given its ability to guide nanostructure formation, it likely undergoes conformational adjustments to optimize Pt-{111} interactions.[62]

These three well-characterized platinum-binding peptides share some common physicochemical properties yet reveal distinct differences in sequence composition, charge distribution, and interaction mechanisms. All three peptides contain polar amino acids, facilitating hydrogen bonding and electrostatic interactions with platinum surfaces, but differ in hydrophobicity, aromatic content, and metal-coordinating residues, which drive their facet preferences. T7 and S7 share serine (S) and threonine (T) residues, suggesting a role of hydroxyl groups in adsorption, yet T7 is more hydrophobic due to leucine (L), whereas S7 features aromatic phenylalanine (F) and polar glutamine (Q), which promote selective Pt-{111} binding through π–π stacking and

Research Article
doi.org/10.1002/ejic.202500224

hydrogen bonding. BP7a contains one histidine (H), a strong metal-coordinating residue, which enables direct interactions with Pt ions and plays a crucial role in twin-plane stabilization during nanoparticle growth.

The newly identified peptide TG7 (TGELSQK) shows differences in amino acid composition compared to the other three well-known platinum-binding sequences. TG7 contains a higher proportion of charged and polar residues, including glutamic acid (E), lysine (K), and glutamine (Q), which suggests a stronger electrostatic and hydrogen bonding contribution to its adsorption behavior. The presence of serine (S) introduces hydroxyl functionality. However, the absence of hydrophobic and aromatic residues may indicate a different adsorption mechanism. Compared to T7, which was also identified on a Pt-{100} target, TG7 stands out due to its more hydrophilic and charged nature. The higher charge density in TG7 (E, K) suggests that electrostatic interactions could play a larger role in its binding to platinum, in contrast to T7's reliance on hydrophobic interactions and hydroxyl-mediated binding. Unlike S7 and BP7a, which contain aromatic residues contributing to π–π stacking with Pt surfaces, TG7 lacks these interactions.

The newly identified peptide L7 (LLVTSVT) exhibits a distinct sequence composition compared to previously known platinum-binding peptides, featuring a high proportion of hydrophobic residues, particularly leucine (L) and valine (V). This strong hydrophobic character suggests a different adsorption mechanism compared to peptides like S7 and BP7a, which rely more on polar and aromatic interactions. The presence of serine (S) and threonine (T) introduces hydroxyl functionalities, which may contribute to hydrogen bonding and surface interactions, like T7 and S7. However, L7 lacks any charged residues, which distinguishes it from TG7, T7, and BP7a, making it less likely to engage in electrostatic interactions with the Pt surface.

Intrinsic conformational propensities for the backbones of amino acids may play a role in the structural adaptability at the bio–inorganic interface. While some residues, such as leucine (L) and valine (V), promote compact, hydrophobic-driven interactions, others—such as serine (S), threonine (T), glutamine (Q), and lysine (K)—are associated with increased backbone flexibility.[63–66] Within the five peptides, we observe a spectrum of disorder- or order-promoting residues that may influence their adsorption. The T7 and S7 peptides, for instance, contain multiple hydroxylated residues (serine and threonine), which are known to enhance surface interactions while maintaining conformational flexibility. Similarly, TG7 incorporates both glutamic acid (E) and lysine (K), which contribute to electrostatic interactions while also promoting a more disordered conformational ensemble. In contrast, L7 is enriched in leucine (L) and valine (V), residues that typically favor hydrophobic clustering and a less flexible structural arrangement. The histidine (H) residue of the BP7A peptide can engage in metal coordination and contributes to local conformational adjustments based on the protonation state.[63] These intrinsic conformational tendencies, coupled with interfacial interactions, may dictate how each peptide reorganizes upon adsorption. To further investigate how these peptides interact with platinum surfaces, we next examined their adsorption behavior and binding affinities using QCM-D measurements before investigating conformational changes upon interaction with Pt nanoparticles using SRCD spectroscopy.

2.2. Adsorption Kinetics and Binding Affinities of Pt-Binding Peptides

While sequence composition and facet specificity provide hints toward potential binding mechanisms, a direct comparison of the peptides is necessary to assess their interaction strength with platinum. QCM-D was selected for evaluating peptide adsorption onto platinum because it provides real-time, label-free insights into both mass uptake and viscoelastic properties of adsorbed layers. Unlike other methods, QCM-D distinguishes between viscoelastic differences in the peptide layer which may reflect underlying enthalpic and entropic contributions to the binding: rigid layers often correlate with enthalpically driven, stronger direct interactions, whereas more flexible layers could indicate significant entropic contributions.[67,68] The commercially available sensor used in this study consists of polycrystalline platinum, predominantly exposing the {111} plane (see S3, Supporting Information).

The time-dependent adsorption behavior of the five investigated PtBPs was systematically analyzed using four different concentrations for each peptide, ranging typically from 25 μg mL^{-1} to 100 μg mL^{-1}, adapted individually for each peptide. The observed changes in oscillation frequency ($-\Delta f$, third overtone) associated with peptide adsorption onto the Pt sensor surface were recorded as a function of time (sensograms, **Figure 2**, left panels). The sensograms show inverted frequency changes plotted over time, with the maximum frequency shifts for the highest concentrations tested ranging from ≈1.8 s^{-1} to 6 s^{-1} after 600 s.

Typically, such frequency data are analyzed using Langmuir isotherms to determine kinetic binding constants.[69] However, Langmuir isotherms assume uniform monolayer formation and are thus unsuitable for accurately modeling multilayer formation scenarios, where peptide–surface and peptide-–peptide interactions may vary considerably in strength.[69] Therefore, we adopted a linear fitting approach to the frequency change within the first 120 s after peptide adsorption initiation, except for the peptide BP7a (see Figure 2). Each adsorption profile was analyzed using Origin to perform linear regression, obtaining the observed rate constant (k_{obs}). Subsequently, k_{obs} values were plotted as a function of peptide concentration, from which the association (k_a) and dissociation (k_d) constants were derived as the slope and intercept, respectively (Figure 2, right panels).[67,69,70] From these values, the equilibrium dissociation constants ($K_D = k_d/k_a$) and the Gibbs free energies of adsorption ($\Delta G = RT \ln (K_{eq} \cdot \nu_s)$) were also calculated (see **Table 2**).[67,70] A comparison of Langmuir adsorption fits and linear initial-rate fits for all peptide–concentration combinations is provided in the Supporting Information (Figure S4-1, Supporting Information). This analysis shows that the linear fit achieved higher Corr. R^2 values than the Langmuir model in most cases, supporting its use for quantifying initial adsorption rates.

For some peptides, low dissipation shifts ($<10^{-6}$) were observed on adsorption (Figure 2) which indicated that rigid films were formed.[67,71–74] For these peptides, the changes in frequency

Research Article
doi.org/10.1002/ejic.202500224

Chemistry Europe
European Chemical Societies Publishing

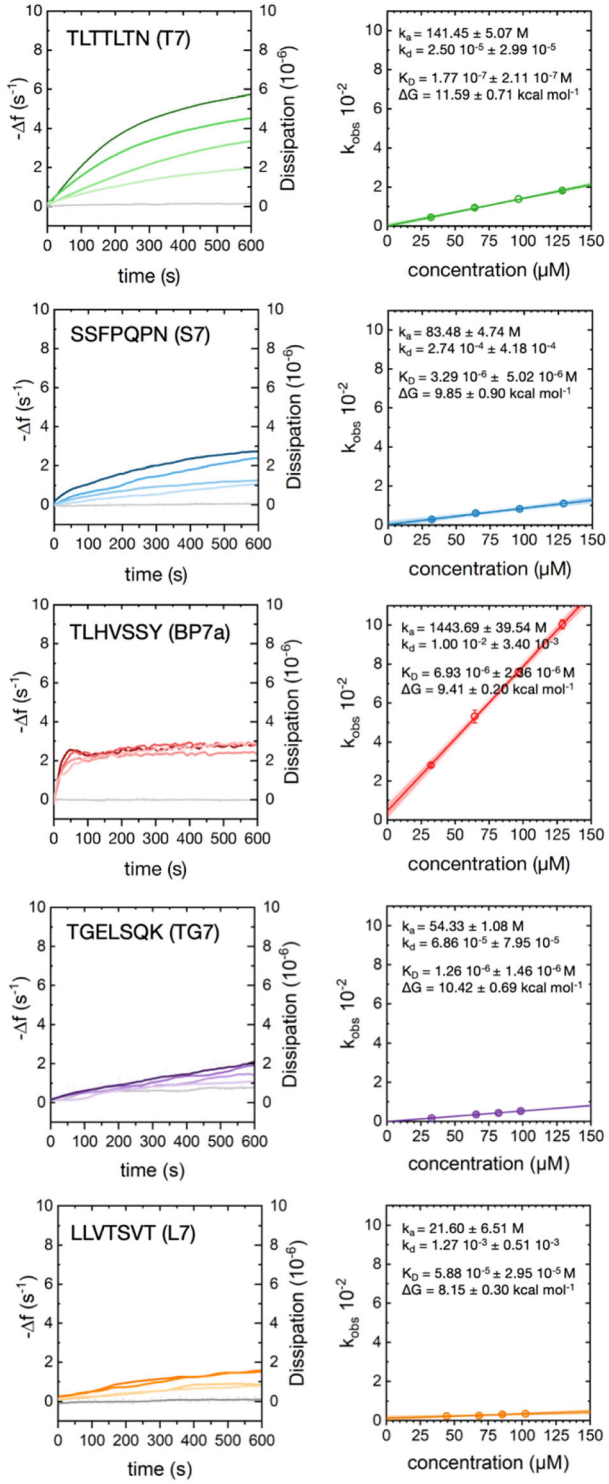

Figure 2. QCM-D measured third overtone changes in oscillation frequency ($-\Delta f$) for the adsorption of the five peptides to Pt sensor. The frequency changes are inverted and plotted against time. Right panels show the determined k_{obs} values for the different peptide concentrations obtained by a linear fitting of the data in the left panel.

of the oscillating sensor at the third overtone could directly be correlated to the mass of adsorbed adlayer by applying the Sauerbrey equation ($\Delta m = -17.7^* \Delta f/3$, see SI4).[72,74,75] However, it is important to note that the measured mass coupled to the surface includes added mass due to peptide hydration and entrapment of solvent molecules.[73,74,76]

The T7 peptide (TLTTLTN) exhibited the strongest overall affinity toward the platinum {111} sensor surface in this study. The QCM-D sensograms display a smooth adsorption profile with plateau indications at higher concentrations. Frequency shifts for the different concentrations tested ranged from ≈2 s^{-1} to 6 s^{-1} after 600 s. Dissipation values remained consistently low ($<10^{-6}$), indicating the formation of a rigid, well-ordered peptide adlayer. Kinetic fitting revealed a high association rate constant ($k_a = 141.45 \pm 5.07\ M^{-1}\ s^{-1}$) and a low dissociation rate ($k_d = 2.50 \times 10^{-5} \pm 2.99 \times 10^{-5}\ s^{-1}$), resulting in a dissociation constant K_D of 1.77×10^{-7} M and a binding free energy of -11.59 ± 0.71 kcal mol^{-1}, the most negative among all five peptides tested. The strong binding is consistent with the peptide's sequence, where threonine residues provide hydroxyl groups for polar interactions and leucines contribute hydrophobic stabilization. Together, these interactions likely result in a densely packed adlayer with high order and facet-adaptive surface engagement.

The S7 peptide (SSFPQPN) demonstrated moderate but consistent adsorption behavior on the platinum {111} sensor in this study. QCM sensograms showed a gradual increase in adsorbed mass across the tested concentrations, leading to a plateau, indicative of slower adsorption kinetics compared to T7. Frequency shifts for the different concentrations tested ranged from ≈1.5 s^{-1} to 3 s^{-1} after 600 s. Dissipation values remained low ($<10^{-6}$), suggesting the formation of a stable, rigid peptide adlayer. Kinetic analysis yielded an association rate constant of $83.48 \pm 4.74\ M^{-1}\ s^{-1}$ and a dissociation rate of $2.74 \times 10^{-4} \pm 4.18 \times 10^{-4}\ s^{-1}$, resulting in a K_D of 3.29×10^{-6} M and a binding free energy of -9.85 ± 0.90 kcal mol^{-1}, placing S7 in the middle range among the peptides tested. The binding is likely governed by the phenylalanine residue, which enables π–π stacking with the platinum surface, alongside polar interactions contributed by serine, glutamine, and asparagine. Despite its facet specificity, S7 binds less strongly than T7 on the Pt-{111} surface, likely due to the absence of hydrophobic clustering and synergistic multiresidue anchoring that characterizes T7's "dual-mode" interaction strategy.

The BP7a peptide (TLHVSSY) exhibited rapid and high-affinity adsorption behavior on the Pt {111} surface. QCM-D frequency curves revealed an immediate drop upon injection, with adsorption reaching a stable plateau within the first 60 s, indicative of fast surface engagement. Frequency shifts for the different concentrations tested ranged from ≈2.5 s^{-1} to 3 s^{-1} after 600 s. The association rate constant ($k_a = 1443.69 \pm 39.54\ M^{-1}\ s^{-1}$) was the highest among all peptides tested, consistent with the presence of a histidine residue that likely coordinates directly with platinum atoms. Despite this rapid association, the peptide also exhibited the highest dissociation rate ($k_d = 1.00 \times 10^{-2} \pm 3.40 \times 10^{-3}\ s^{-1}$), leading to a moderate overall binding affinity ($K_D = 6.93 \times 10^{-6}$ M) and a free energy of adsorption of -9.41 ± 0.20 kcal mol^{-1}. Dissipation values remained low throughout the adsorption process, suggesting that BP7a forms a rigid and well-ordered adlayer. While histidine

Research Article
doi.org/10.1002/ejic.202500224

Table 2. Summary of thermodynamic parameters for the five investigated binding peptides interacting with platinum {111} using QCM-D.

Sequence	TLTTLTN (T7)	SSFPQPN (S7)	TLHVSSY (BP7A)	TGELSQK (TG7)	LLVTSVT (L7)
k_a	141.45 ± 5.10	83.48 ± 4.74	1443.69 ± 39.94	54.33 ± 1.08	21.6 ± 6.51
k_d 10^{-6}	25.0 ± 29.9	275 ± 4.18	10,000 ± 3,400	1.26 ± 1.46	1,270 ± 510
K_D (10^{-7} M)	1.77 ± 2.11	32.9 ± 50.2	69.3 ± 23.6	12.6 ± 14.6	588 ± 259
ΔG (kcal mol^{-1})	−11.59 ± 0.71	−9.85 ± 0.90	−9.41 ± 0.20	−10.42 ± 0.69	−8.15 ± 0.30

likely dominates the initial metal–binding interaction, the peptide's relatively low hydrophobic content and absence of multipoint anchoring may reduce lateral stabilization on the surface, resulting in higher desorption and lower net affinity compared to more synergistic binders like T7.

The TG7 peptide (TGELSQK) demonstrated strong and stable adsorption behavior on the platinum {111} surface. Frequency shifts for the different concentrations tested ranged from ≈1.5 s^{-1} to 2 s^{-1} after 600 s. The QCM-D sensograms showed a slow but steady increase in adsorbed mass over time, indicative of gradual surface association. Despite its moderate association rate ($k_a = 54.33 \pm 1.08\ M^{-1}\ s^{-1}$), TG7 displayed a remarkably low dissociation rate ($k_d = 6.86 \times 10^{-5} \pm 7.95 \times 10^{-5}\ s^{-1}$), yielding a dissociation constant of 1.26×10^{-6} M and a free energy of −10.42 ± 0.69 kcal mol^{-1} - the second most negative value among all peptides tested. Unlike the other peptides, TG7 exhibited the highest dissipation shift, suggesting a more viscoelastic or loosely packed adlayer. This may reflect conformational mobility or limited lateral interactions due to its high content of polar and charged residues. The peptide's strong affinity is likely driven by electrostatic interactions from glutamic acid and lysine, and hydrogen bonding via serine and glutamine. Although originally identified on a Pt-{100} target, TG7 binds strongly to Pt {111} surfaces, demonstrating that electrostatic anchoring can provide robust interactions even in the absence of hydrophobic stabilization.

The L7 peptide (LLVTSVT) exhibited the weakest overall interaction with the platinum {111} sensor. QCM-D frequency shifts were small and increased only gradually, consistent with slow and limited surface binding. The association rate constant ($k_a = 21.60 \pm 6.51\ M^{-1}\ s^{-1}$) was the lowest among all peptides tested, while the relatively high dissociation rate ($k_d = 1.27 \times 10^{-3} \pm 0.51 \times 10^{-3}\ s^{-1}$) further contributed to its poor affinity. This resulted in a dissociation constant K_D of 5.88×10^{-5} M and a binding free energy of –8.15 ± 0.30 kcal mol^{-1}, the least negative of the group. Although dissipation values remained low, their gradual increase suggests the formation of a somewhat less rigid adlayer in comparison to T7, S7, and BP7a. The peptide's high hydrophobic content, comprising primarily leucine and valine residues, supports a binding mechanism dominated by weak van der Waals and hydrophobic interactions. However, the absence of charged or aromatic residues likely limits specific recognition or strong adsorption to the Pt {111} surface, making L7 a relatively poor binder in this context.

In summary, our QCM-D analysis reveals that the five platinum-binding peptides differ markedly in their adsorption kinetics and the viscoelastic properties of the resulting adlayers. The overall affinity trend: T7 > TG7 > S7 > BP7a > L7 reflects the combined contributions of polar, hydrophobic, and aromatic residues to surface binding. T7 and S7 form rigid, well-ordered films with low dissipation shifts, while TG7, despite its strong affinity, shows the highest dissipation, indicative of a more flexible or hydrated peptide layer. BP7a exhibits a rapid adsorption profile with moderate dissociation, whereas L7 shows weak binding and a gradual increase in dissipation, consistent with a loosely packed adlayer. These findings fall within the expected range of Pt-binding peptide affinities reported in the literature[2,23] and highlight how residue-specific interactions shape peptide behavior at the interface. Consistent with its lower facet specificity, the peptide selected on the polycrystalline Pt target showed the weakest binding affinity, effectively serving as an internal reference for less optimized binders. However, the observed differences are likely not solely due to binding side chains. The inherent conformational backbone preferences and structural adaptability of the peptides, based on their primary structure, may also represent an important contributing factor in governing their interfacial organization, as discussed in the following section.

2.3. Conformational Changes in Pt-Binding Peptides upon Adsorption

SRCD spectroscopy was used to investigate the conformational properties of the platinum-binding peptides in solution and to assess potential conformational changes upon interaction. Due to absorption and scattering effects from the nanoparticles, the wavelength region below 190 nm was not accessible using a standard CD instrument, necessitating the use of SRCD to extend the spectral range.

The SRCD spectra of binding peptides, both in solution and upon interaction with platinum nanoparticles, reveal predominantly unordered conformational ensembles (**Figure 3**). These structures have a pronounced minimum between 195 nm and 200 nm and a weak maximum between 210 nm and 220 nm.[77] While all peptides exhibit characteristic CD signatures indicative of a disordered conformational ensemble in solution, their adsorption onto cubic and octahedral platinum nanoparticles induces notable conformational changes (see Figure 3 middle and far-right columns of data). However, attempts to quantitatively resolve these conformational changes using state-of-the-art secondary structure analysis tools (BeStSel[78,79]) have been inconclusive (see S5, Supporting Information), as the observed spectral variations remain within the expected fitting deviation. CD

Research Article
doi.org/10.1002/ejic.202500224

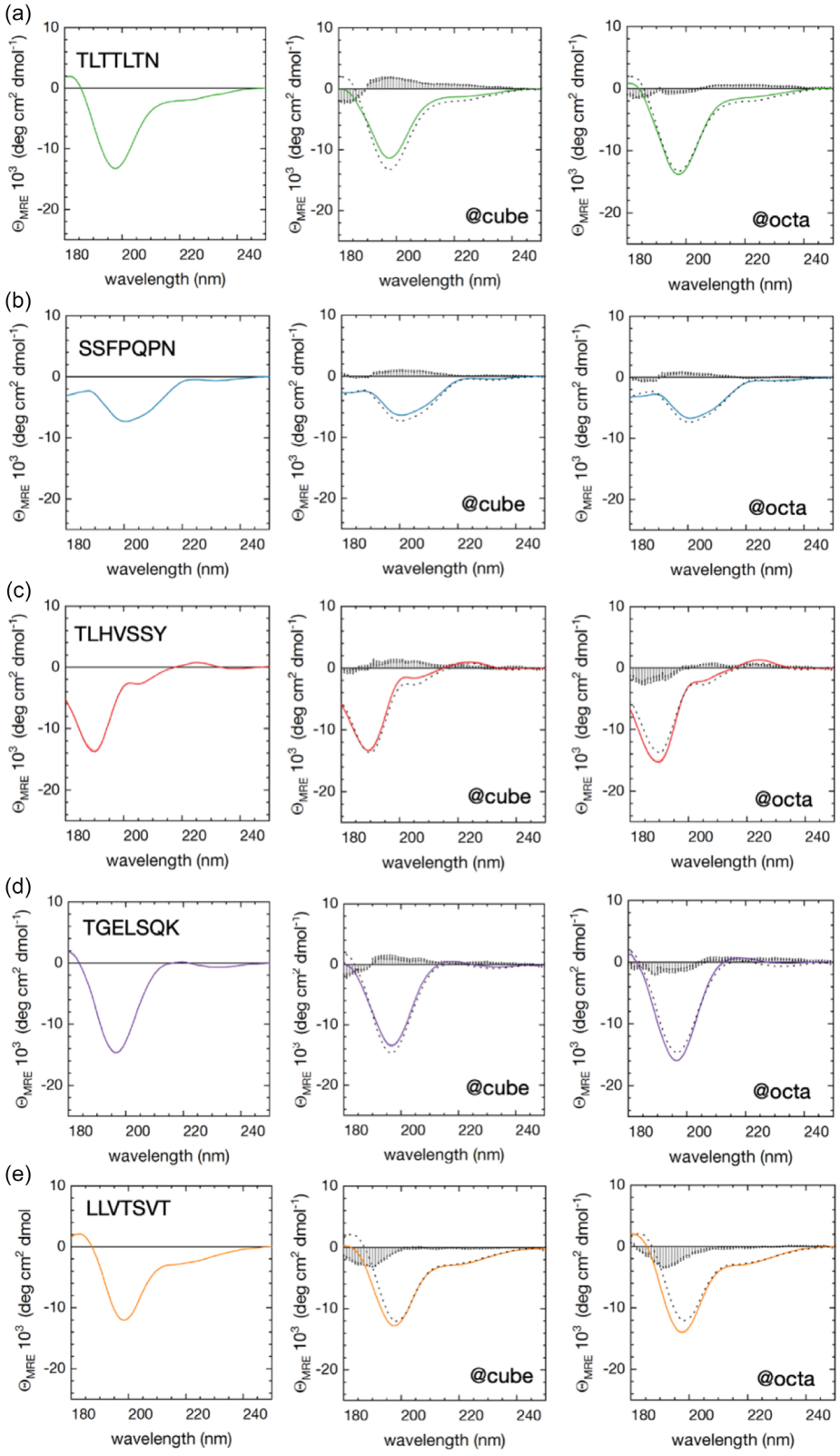

Figure 3. Comparison of the CD spectra of five platinum binding peptides in ddH_2O and upon interaction with different platinum nanoparticle morphologies. Left panel showing the CD spectra of the five investigated PtBPs in ddH_2O. Mid-panel and right panel show PtBPs conformational changes upon adsorption on Pt cubes and the conformational changes upon adsorption on Pt octahedras, respectively. The dashed line corresponds to the measurement in ddH_2O, and the bars are indicating the differences between the two spectra. All spectra are averaged from three scans after baseline subtraction, the shaded areas indicate the deviations. These measurements were performed at the DISCO Beamline (Synchrotron Soleil).

Research Article
doi.org/10.1002/ejic.202500224

spectroscopy measures a macroscopic signal that represents a linear combination of numerous fluctuating microstates. Due to the flat and less structured free energy landscape typical of disordered systems, a multitude of conformers contribute to the measured signal, making secondary structure deconvolution inherently uncertain. Without extensive sampling of representative conformers for example, through enhanced molecular simulations, it is difficult to fully characterize the conformational ensemble and the conditional order present within the system.[51] Nonetheless, the facet-dependent spectral shifts observed across all peptides strongly support the presence of genuine conformational adaptation upon adsorption.

In solution, the CD spectrum of T7 is defined by a prominent negative band between 195 and 200 nm, a negative shoulder around 220 nm, and positive ellipticity at 180 nm. This spectral profile indicates a predominantly unstructured conformation, with contributions from antiparallel β-sheet components and turns, as identified by BeStSel analysis (see S5, Supporting Information). Upon adsorption onto cubic platinum nanoparticles ({100} facets), the intensity of the negative band between 195 and 200 nm decreases, while the ellipticity at 180 nm becomes slightly negative, approaching 0. In contrast, adsorption onto octahedral platinum nanoparticles results in only minor spectral changes, with slight variations in ellipticity but an overall preservation of the solution-state spectral shape. Although T7 retains positive ellipticity at 180 nm upon binding to octahedral Pt surfaces, its intensity is significantly reduced compared to the solution spectrum. These results suggest that T7 undergoes more pronounced conformational changes upon interaction with cubic Pt nanoparticles, aligning with its original identification on {100} facets.[23]

In solution, the CD spectrum of S7 displays a broad minimum centered around 200 nm, along with a wide shoulder and a smaller minimum near 230 nm. Additionally, a flex point appears at 188 nm, and the ellipticity remains negative at 180 nm, indicating a largely unordered conformation with contributions primarily from antiparallel β-sheet components and turns (see S5, Supporting Information). Upon adsorption onto cubic platinum nanoparticles, the overall spectral shape remains largely unchanged, with a reduction in mean residue ellipticity at 200 nm. A similar trend is observed upon interaction with octahedral platinum nanoparticles, where the spectrum remains mostly consistent with the solution state, but with a further reduction in mean residue ellipticity at 200 nm and additional changes around the 188 nm flex point. Overall, S7 undergoes only subtle conformational changes upon adsorption, with minimal spectral differences between its interactions with cubic and octahedral platinum nanoparticles. However, the slightly stronger spectral changes observed upon adsorption onto octahedral nanoparticles are in line with its original identification on {111} facets, which are prominently displayed by the surfaces of octahedral platinum nanoparticles.[23]

In solution, BP7a exhibits a CD spectrum characterized by a pronounced minimum at 190 nm, a maximum between 220 and 230 nm, and a shoulder around 205 nm. Additionally, the ellipticity remains negative at 180 nm, indicating a predominantly disordered conformation with contributions from antiparallel β-sheets and turns (see S5, Supporting Information). Upon adsorption onto cubic platinum nanoparticles, the overall spectral shape remains largely unchanged, with slight differences in the shoulder region, where the intensity is reduced. In contrast, adsorption onto octahedral platinum nanoparticles leads to more pronounced changes, including an increase in the intensity of the minimum at 190 nm, modifications in the shoulder region, and an increase in the maximum between 220 and 230 nm. These observations suggest that BP7a undergoes stronger conformational changes upon interaction with octahedral platinum nanoparticles, which aligns with its previously reported preferential adsorption toward the Pt-{111} facet, where it plays a role in stabilizing single-twinned seeds and promoting multipod formation during Pt nanoparticle synthesis.[20]

In solution, the CD spectrum of TG7 is characterized by a pronounced minimum between 195 and 200 nm, positive values near 220 nm, a slight minimum around 230 nm, and positive ellipticity at 180 nm, indicating a largely disordered conformation with contributions from antiparallel β-sheets and turns (see S5, Supporting Information). Upon adsorption onto cubic platinum nanoparticles, the spectrum shows a reduction in the ellipticity of the main minimum, and the intensity at 180 nm decreases almost to 0. In contrast, adsorption onto octahedral platinum nanoparticles results in an increase in the intensity of the main minimum, while the maximum around 220 nm becomes more pronounced. These observations suggest that TG7 undergoes facet-dependent conformational adjustments upon adsorption. Given that TG7 was originally identified on {100} targets within this work, its spectral response on cubic Pt nanoparticles may indicate a greater degree of structural rearrangement, whereas the changes observed upon interaction with octahedral nanoparticles likely reflect a different mode of structural adaptation.

In solution, the CD spectrum of L7 exhibits a prominent negative band between 195 and 200 nm, a negative shoulder around 220 nm, and positive ellipticity at 180 nm, suggesting a largely disordered conformation with contributions from antiparallel β-sheet components and turns (see S5, Supporting Information). Upon adsorption onto cubic platinum nanoparticles, the spectrum undergoes a slight shift of the minimum toward lower wavelengths, accompanied by an increase in signal intensity. Additionally, the positive ellipticity at 180 nm decreases, approaching zero. Adsorption onto octahedral platinum nanoparticles results in a comparatively stronger increase in the intensity of the minimum, while the spectral shift to lower wavelengths remains consistent. However, unlike in the cubic case, the ellipticity at 180 nm is retained. These observations suggest that L7 undergoes conformational adjustments upon adsorption, with more pronounced spectral changes observed on octahedral platinum nanoparticles. Given that L7 was originally identified on a polycrystalline platinum target within this study, its ability to adapt to different surface facets may contribute to these adsorption-dependent spectral variations.

The CD spectra of all investigated platinum-binding peptides in solution indicate predominantly unordered conformations. Contributions from antiparallel β-sheets and turns are observed in all peptides to different extents. As discussed above, structural flexibility is a known feature of peptides that interact with solid

Research Article
doi.org/10.1002/ejic.202500224

surfaces, potentially enabling conformational adaptation upon adsorption.[52–54] Overall, peptides identified on {100} facets (T7, TG7) exhibit more pronounced conformational changes upon adsorption onto cubic Pt nanoparticles, whereas S7, which was identified on {111} facets, shows greater spectral variations on octahedral Pt surfaces. Similarly, BP7a, although originally identified on Pt nanowires, has been previously reported to exhibit a strong preference for {111} facets, which aligns with the conformational changes observed upon adsorption onto octahedral Pt nanoparticles.

We have successfully established a procedure to measure conformational changes of proteins and peptides upon interaction with nanoparticles and at oil–water interfaces in previous studies.[50,80–82] However, we recognize the possibility that partial desorption of peptides may occur upon resuspension of the nanoparticles before the CD measurement begins. While this remains a potential limitation, we confirmed that no further spectral changes were observed across three consecutive measurements, indicating that the system had stabilized within the measurement timeframe. Nevertheless, it cannot be excluded that the measured spectra reflect a mixture of adsorbed and desorbed peptides, making the observed spectral differences even more remarkable. Given the high costs associated with both peptides and nanoparticles, dedicated desorption studies were not feasible, yet the observed facet-dependent spectral variations strongly support the presence of distinct adsorption-induced conformational changes.

3. Conclusion and Outlook

In this study, we conducted a comprehensive, side-by-side analysis of five platinum-binding peptides, three known and two newly identified, using QCM-D and SRCD spectroscopy to investigate their adsorption behavior and conformational properties on Pt surfaces. Our QCM-D results revealed distinct kinetic profiles and binding affinities, with T7 and TG7 exhibiting the strongest overall interactions and L7 the weakest. Notably, differences in dissipation shifts correlated with the rigidity or viscoelasticity of the adsorbed peptide layers, offering insight into the enthalpic versus entropic contributions to binding.

SRCD analysis further revealed that all peptides adopt predominantly disordered conformations in solution yet undergo facet-dependent conformational changes upon adsorption. These structural adjustments were most pronounced for peptides binding to their "matched" facets, as defined by their PD origin. Despite the limitations of secondary structure deconvolution for disordered peptides, consistent spectral shifts across nanoparticle morphologies support the presence of genuine conformational adaptation at the interface.

Together, our findings highlight how sequence composition, conformational flexibility, and interfacial recognition collectively govern Pt–PtBP interactions. This integrated approach provides a first step toward a framework for understanding peptide–surface interactions in greater molecular detail and may support the rational design of peptides as bioinspired SDAs for nanomaterials and catalytic surfaces. However, to gain a more fundamental understanding of peptide interactions during a biomineralization route, an important aspect to consider is the impact of the pH of the environment. pH is an important variable that can modulate not only the binding strength and facet preference of Pt-binding peptides, but also their conformation.

It is well known that pH decreases during Pt nanocrystal synthesis due to proton release from reducing agents such as $NaBH_4$[83] and certain Pt-binding peptides have been reported to lose strong binding under pH modulation.[20] Previous studies have shown that pH can influence peptide–Pt interactions by altering the protonation states of side chains directly involved in coordination, thereby affecting both adsorption affinity and the resulting nanocrystal morphology.[20,83–85] In peptide-templated Pt deposition, histidine-containing sequences have shown pH-dependent coordination modes: under acidic conditions (pH 4) binding occurs via the carboxylate oxygen of histidine to Pt^{2+}, whereas under basic conditions (pH 10) coordination through the imidazole nitrogen is favored, enabling more uniform Pt coatings.[84] Such pH-driven changes in binding mode are coupled to protonation-dependent shifts in the peptide's conformational ensemble, a phenomenon well documented for amino acids and peptides in solution.[63–65]

While pH effects were not investigated in the present work, our SRCD results demonstrate that Pt-binding peptides can undergo measurable, facet-dependent conformational adjustments upon adsorption. Since protonation state changes are well known to modulate intramolecular interactions and hydrogen-bonding networks in peptides, pH variation could similarly shift the conformational ensemble at the interface, thereby influencing both adsorption strength and structural adaptability. Exploring these effects through controlled pH variation represents a promising avenue for future studies.[87–88]

Acknowledgements

Funding from AFOSR FA9550-13-1-0040 and FA9550-24-1-0274 is gratefully acknowledged. The CD spectra were obtained at the DISCO Beamline at Synchrotron Soleil (Proposal 220181468 "Interfacial Conformations: from nanoparticles to metal-organic frameworks") with support from beamline Scientist Frank Wien and beamline manager Matthieu Réfrégiers. The authors thank Andrew J. Organisciak and Danielle Carson for their contributions in the preliminary QCM-D studies.

Conflict of Interest

The authors declare no conflict of interest.

Author Contributions

Monika Michaelis: conceptualization (supporting); data curation (lead); formal analysis (lead); funding acquisition (supporting); investigation (equal); methodology (equal); supervision (supporting);

visualization (equal); writing—original draft (lead); writing—review & editing (equal). **Marion J. Limo**: data curation (supporting); investigation (supporting); supervision (supporting); writing—review & editing (supporting). **Swetha R. Kothur**: data curation (supporting); investigation (supporting); methodology (supporting). **Carole C. Perry:** conceptualization (lead); data curation (supporting); formal analysis (equal); funding acquisition lead; project administration (lead); resources (lead); supervision (lead); validation (equal); writing—original draft (supporting); writing—review & editing (equal).

Data Availability Statement

The data that support the findings of this study are available in the supplementary material of this article.

Keywords: binding free energy · circular dichroism spectroscopy · conformational changes · platinum binding peptides · quartz crystal microbalance with dissipation monitoring

[1] M. Han, K. Kani, J. Na, J. Kim, Y. Bando, T. Ahamad, S. M. Alshehri, Y. Yamauchi, *Adv. Funct. Mater.* **2023**, *33*, https://doi.org/10.1002/adfm.202301831.
[2] N. Pramounmat, K. Yan, J. Wolf, J. N. Renner, *Multifunct. Mater.* **2022**, *5*, https://doi.org/10.1088/2399-7532/ac4a86.
[3] A. Chen, P. Holt-Hindle, *Chem. Rev.* **2010**, *110*, 3767.
[4] R. Huang, Y.-H. Wen, Z.-Z. Zhu, S.-G. Sun, *J. Mater. Chem.* **2011**, *21*, 11578.
[5] Y. Liu, E. Zhu, J. Huang, A. Zhang, A. H. Shah, Q. Jia, M. Xu, E. Liu, Q. Sun, X. Duan, Y. Huang, *Nano Lett.* **2023**, *23*, 2758.
[6] C. M. Zalitis, A. R. Kucernak, J. Sharman, E. Wright, *J. Mater. Chem. A Mater.* **2017**, *5*, 23328.
[7] E. Zhu, X. Yan, S. Wang, M. Xu, C. Wang, H. Liu, J. Huang, W. Xue, J. Cai, H. Heinz, Y. Li, Y. Huang, *Nano Lett.* **2019**, *19*, 3730.
[8] X. Li, G. Li, W. Zang, L. Wang, X. Zhang, *Catal. Sci. Technol.* **2014**, *4*, 3290.
[9] A. Šulce, J. Backenköhler, I. Schrader, M. D. Piane, C. Müller, A. Wark, L. C. Ciacchi, V. Azov, S. Kunz, *Catal. Sci. Technol.* **2018**, *8*, 6062.
[10] S. Y. Gutiérrez de la Rosa, R. Muñiz Diaz, P. T. Villalobos Gutiérrez, R. Patakfalvi, Ó. Gutiérrez Coronado, *Int. J. Mol. Sci.* **2022**, *23*, 9404.
[11] E. O. Mikhailova, *J. Funct. Biomater.* **2022**, *13*, 260.
[12] N. V. Long, N. D. Chien, T. Hayakawa, H. Hirata, G. Lakshminarayana, M. Nogami, *Nanotechnology* **2010**, *21*, 035605.
[13] Z. Peng, H. Yang, *Nano Today* **2009**, *4*, 143.
[14] J. J. De Yoreo, P. G. Vekilov, *Biomineralization*, De Gruyter **2003**, pp. 57–94.
[15] Y. Song, S. R. Challa, C. J. Medforth, Y. Qiu, R. K. Watt, D. Peña, J. E. Miller, F. van Swol, J. A. Shelnutt, *Chem. Commun.* **2004**, 1044.
[16] L. M. Forbes, A. P. Goodwin, J. N. Cha, *Chem. Mater.* **2010**, *22*, 6524.
[17] J. W. Gibbs, *Am. J. Sci.* **1878**, *s3-16*, 441.
[18] A. R. Tao, S. Habas, P. Yang, *Small* **2008**, *4*, 310.
[19] H. Song, F. Kim, S. Connor, G. A. Somorjai, P. Yang, *J. Phys. Chem. B* **2005**, *109*, 188.
[20] Y. Li, G. P. Whyburn, Y. Huang, *J. Am. Chem. Soc.* **2009**, *131*, 15998.
[21] A. R. Bassindale, A. Codina-Barrios, N. Frascione, P. G. Taylor, *Chem. Commun.* **2007**, 2956.
[22] E. Dujardin, C. Peet, G. Stubbs, J. N. Culver, S. Mann, *Nano Lett.* **2003**, *3*, 413.
[23] C. Y. Chiu, Y. Li, L. Ruan, X. Ye, C. B. Murray, Y. Huang, *Nat. Chem.* **2011**, *3*, 393.
[24] Q. Li, Y. Wang, G. Zhang, R. Su, W. Qi, *Chem. Soc. Rev.* **2023**, *52*, 1549.
[25] T. N. Vigil, L. C. Spangler, *ACS Appl. Nano Mater.* **2023**, https://doi.org/10.1021/acsanm.3c04277.
[26] T. Yang, Y. Shi, A. Janssen, Y. Xia, *Angew. Chem. Int. Ed.* **2020**, *59*, 15378.
[27] L. Addadi, D. Joester, F. Nudelman, S. Weiner, *Chem. – A Eur. J.* **2006**, *12*, 980.
[28] M. B. Dickerson, K. H. Sandhage, R. R. Naik, *Chem. Rev.* **2008**, *108*, 4935.
[29] C. Y. Chiu, L. Ruan, Y. Huang, *Chem. Soc. Rev.* **2013**, *42*, 2512.
[30] C. C. Perry, S. V. Patwardhan, O. Deschaume, *Biochem. Soc. Trans.* **2009**, *37*, 687.
[31] K. Sanford, M. Kumar, *Curr. Opin. Biotechnol* .**2005**, *16*, 416.
[32] A. Veis, A. Perry, *Biochemistry* **1967**, *6*, 2409.
[33] G. P. Smith, *Science 1979* **1985**, *228*, 1315.
[34] G. P. Smith, V. A. Petrenko, *Chem. Rev.* **1997**, *97*, 391.
[35] G. P. Smith, *Angew. Chem. Int. Ed.* **2019**, *58*, 14428.
[36] M. Sarikaya, C. Tamerler, A. K.-Y. Jen, K. Schulten, F. Baneyx, *Nat. Mater.* **2003**, *2*, 577.
[37] R. R. Naik, L. L. Brott, S. J. Clarson, M. O. Stone, *J. Nanosci. Nanotechnol.* **2002**, *2*, 95.
[38] E. E. Oren, C. Tamerler, M. Sarikaya, *Nano Lett.* **2005**, *5*, 415.
[39] K.-I. Sano, H. Sasaki, K. Shiba, *Langmuir* **2005**, *21*, 3090.
[40] M. M. Tomczak, M. K. Gupta, L. F. Drummy, S. M. Rozenzhak, R. R. Naik, *Acta Biomater.* **2009**, *5*, 876.
[41] D. Rothenstein, B. Claasen, B. Omiecienski, P. Lammel, J. Bill, *J. Am. Chem. Soc.* **2012**, *134*, 12547.
[42] E. Eteshola, L. J. Brillson, S. C. Lee, *Biomol. Eng.* **2005**, *22*, 201.
[43] L. Ruan, C. Y. Chiu, Y. Li, Y. Huang, *Nano Lett.* **2011**, *11*, 3040.
[44] L. Ruan, H. Ramezani-Dakhel, C. Y. Chiu, E. Zhu, Y. Li, H. Heinz, Y. Huang, *Nano Lett.* **2013**, *13*, 840.
[45] U. O. S. Seker, B. Wilson, D. Sahin, C. Tamerler, M. Sarikaya, *Biomacromolecules* **2009**, *10*, 250.
[46] U. O. S. Seker, B. Wilson, S. Dincer, I. W. Kim, E. E. Oren, J. S. Evans, C. Tamerler, M. Sarikaya, *Langmuir* **2007**, *23*, 7895.
[47] M. Hnilova, E. E. Oren, U. O. S. Seker, B. R. Wilson, S. Collino, J. S. Evans, C. Tamerler, M. Sarikaya, *Langmuir* **2008**, *24*, 12440.
[48] E. E. Oren, R. Notman, I. W. Kim, J. S. Evans, T. R. Walsh, R. Samudrala, C. Tamerler, M. Sarikaya, *Langmuir* **2010**, *26*, 11003.
[49] J. M. Slocik, A. O. Govorov, R. R. Naik, *Nano Lett.* **2011**, *11*, 701.
[50] A. Sola-Rabada, M. Michaelis, D. J. Oliver, M. J. Roe, L. Colombi Ciacchi, H. Heinz, C. C. Perry, *Langmuir* **2018**, *34*, 8255.
[51] M. Michaelis, L. Cupellini, C. Mensch, C. C. Perry, M. Delle Piane, L. Colombi Ciacchi, *Chem. Sci.* **2023**, *14*, 8483.
[52] S. N. Malkov, M. V. Živković, M. V. Beljanski, M. B. Hall, S. D. Zarić, *J. Mol. Model* **2008**, *14*, 769.
[53] S. Costantini, G. Colonna, A. M. Facchiano, *Biochem. Biophys. Res. Commun.* **2006**, *342*, 441.
[54] K. Fujiwara, H. Toda, M. Ikeguchi, *BMC Struct. Biol.* **2012**, *12*, 18.
[55] M. Sarikaya, C. Tamerler, D. T. Schwartz, F. Baneyx, *Annu. Rev. Mater. Res.* **2004**, *34*, 373.
[56] H. Ramezani-Dakhel, L. Ruan, Y. Huang, H. Heinz, *Adv. Funct. Mater.* **2015**, *25*, 1374.
[57] S. K. Ramakrishnan, M. Martin, T. Cloitre, L. Firlej, F. J. G. Cuisinier, C. Gergely, *J. Chem. Inf. Model* **2013**, *53*, 3273.
[58] S. P. Ju, J. W. Su, C. H. Lin, H. Y. Chen, *Appl. Surf. Sci.* **2019**, *471*, 904.
[59] Y. Li, Y. Huang, *Adv. Mater.* **2010**, *22*, 1921.
[60] L. Ruan, H. Ramezani-Dakhel, C. Lee, Y. Li, X. Duan, H. Heinz, Y. Huang, *ACS Nano* **2014**, *8*, 6934.
[61] L. Ruan, E. Zhu, Y. Chen, Z. Lin, X. Huang, X. Duan, Y. Huang, *Angew. Chem. – Int. Ed.* **2013**, *52*, 12577.
[62] K. Tao, J. Wang, Y. Li, D. Xia, H. Shan, H. Xu, J. R. Lu, *Sci. Rep.* **2013**, *3*, https://doi.org/10.1038/srep02565.
[63] D. A. C. Beck, D. O. V. Alonso, D. Inoyama, V. Daggett, *Proc. Natl. Acad. Sci.* **2008**, *105*, 12259.
[64] M. C. Childers, C.-L. Towse, V. Daggett, *Prot. Eng. Design Select.* **2016**, *29*, 271.
[65] C.-L. Towse, J. Vymetal, J. Vondrasek, V. Daggett, *Biophys. J.* **2016**, *110*, 348.
[66] A. Campen, R. M. Williams, C. J. Brown, J. Meng, V. N. Uversky, A. K. Dunker, *Protein Pept. Lett.* **2008**, *15*, 956.
[67] Z. Tang, J. P. Palafox-Hernandez, W. C. Law, Z. E. Hughes, M. T. Swihart, P. N. Prasad, M. R. Knecht, T. R. Walsh, *ACS Nano* **2013**, *7*, 9632.
[68] A. M. Sultan, Z. C. Westcott, Z. E. Hughes, J. P. Palafox-Hernandez, T. Giesa, V. Puddu, M. J. Buehler, C. C. Perry, T. R. Walsh, *ACS Appl. Mater. Interfaces* **2016**, *8*, 18620.
[69] C. Tamerler, E. E. Oren, M. Duman, E. Venkatasubramanian, M. Sarikaya, *Langmuir* **2006**, *22*, 7712.
[70] R. Coppage, J. M. Slocik, H. Ramezani-Dakhel, N. M. Bedford, H. Heinz, R. R. Naik, M. R. Knecht, *J. Am. Chem. Soc.* **2013**, *135*, 11048.
[71] F. Causa, R. Della Moglie, E. Iaccino, S. Mimmi, D. Marasco, P. L. Scognamiglio, E. Battista, C. Palmieri, C. Cosenza, L. Sanguigno, I. Quinto, G. Scala, P. A. Netti, *J. Colloid Interface Sci.* **2013**, *389*, 220.
[72] M. C. Dixon, *J. Biomol. Tech.* **2008**, *19*, 151.
[73] A. Dolatshahi-Pirouz, K. Rechendorff, M. B. Hovgaard, M. Foss, J. Chevallier, F. Besenbacher, *Colloids Surf. B Biointerfaces* **2008**, *66*, 53.

[74] M. Rodahl, F. Höök, C. Fredriksson, C. A. Keller, A. Krozer, P. Brzezinski, M. Voinova, B. Kasemo, *Faraday Discuss.* **1997**, *107*, 229.
[75] G. Sauerbrey, *Z. Phys.* **1959**, *155*, 206.
[76] H. Chen, X. Su, K.-G. Neoh, W.-S. Choe, *Anal. Chem.* **2006**, *78*, 4872.
[77] J. L. S. Lopes, A. J. Miles, L. Whitmore, B. A. Wallace, *Prot. Sci.* **2014**.
[78] A. Micsonai, F. Wien, É. Bulyáki, J. Kun, É. Moussong, Y.-H. Lee, Y. Goto, M. Réfrégiers, J. Kardos, *Nucleic Acids Res.* **2018**, *46*, W315.
[79] A. Micsonai, F. Wien, L. Kernya, Y.-H. Lee, Y. Goto, M. Réfrégiers, J. Kardos, *Proc. Natl. Acad. Sci.* **2015**, 112, https://doi.org/10.1073/pnas.1500851112.
[80] T. Wollborn, M. Michaelis, L. C. Ciacchi, U. Fritsching, *J. Colloid Interface Sci.* **2022**, *628*, 72.
[81] N. Hildebrand, M. Michaelis, N. Wurzler, Z. Li, J. D. Hirst, A. Micsonai, J. Kardos, A. Gil-Ley, G. Bussi, S. Köppen, M. D. Piane, L. C. Ciacchi, *ACS Biomater. Sci. Eng.* **2018**, *4*, 4036.
[82] M. Michaelis, N. Hildebrand, R. H. Meißner, N. Wurzler, Z. Li, J. D. Hirst, A. Micsonai, J. Kardos, M. Delle Piane, L. Colombi Ciacchi, *J. Phys. Chem. B* **2019**, *123*, 6694.
[83] J. Wang, K. Tao, Y. Yang, L. Zhang, D. Wang, M. Cao, Y. Sun, D. Xia, *RSC Adv.* **2016**, *6*, 58099.
[84] L. Yu, I. A. Banerjee, H. Matsui, *J. Mater. Chem.* **2004**, *14*, 739.
[85] J. A. Michel, W. H. Morris III, C. M. Lukehart, *J. Mater. Chem. A Mater.* **2015**, *3*, 2012.
[86] G. E. Crooks, G. Hon, J.-M. Chandonia, S. E. Brenner, *Genome Res.* **2004**, *14*, 1188.
[87] T. D. Schneider, R. M. Stephens, *Nucleic Acids Res.* **1990**, *18*, 6097.
[88] E. Gasteiger, C. Hoogland, A. Gattiker, M. R. Wilkins, R. D. Appel, A. Bairoch, et al., *The Proteomics Protocols Handbook*, Springer **2005**, pp. 571–607.

Manuscript received: April 28, 2025
Revised manuscript received: August 13, 2025
Version of record online: